applied sciences

Article

Phase Transition and Controlled Zirconia Implant Patterning Using Laser-Induced Shockwaves

Inomjon Majidov, Yaran Allamyradov, Salizhan Kylychbekov, Zikrulloh Khuzhakulov and Ali Oguz Er *

Department of Physics & Astronomy, Western Kentucky University, Bowling Green, KY 42101, USA; ima270@uky.edu (I.M.); yaran.allamyradov485@topper.wku.edu (Y.A.); salizhan.kylychbekov837@topper.wku.edu (S.K.); zikrulloh.khuzhakulov949@topper.wku.edu (Z.K.)
* Correspondence: ali.er@wku.edu

Abstract: Zirconia is increasingly favored for dental implants owing to its corrosion resistance, hypoallergenic properties, and superior esthetics, but its biocompatibility remains a challenge. This study explores laser-assisted surface modification to enhance zirconia bioactivity. Zirconia transitions from the monoclinic to the tetragonal phase during sintering, with mixed phases observed in the pre-sintered stage. These transitions are critical for understanding its structural stability and malleability. Grid patterns were imprinted on the green body implant surface using a 1064 nm Nd-YAG laser (Continuum Surelite II, San Jose, CA, USA), with mesh sizes ranging from 7 to 50 μm and depths up to 2 μm, controlled by varying laser fluence, irradiation time, and templates. SEM, AFM, and XRD analyses were used to characterize the surface morphology and crystallography. Protein adsorption studies compared two patterned samples with different surface coverage—the first sample had a patterned area of 0.212 cm^2 (27%), while the second sample had a patterned area of 0.283 cm^2 (36%)—to a control sample. Protein adsorption increased by 92% in the first and 169% in the second sample, demonstrating a direct correlation between increased pattern area and bioactivity. Enhanced protein adsorption facilitates cell attachment and growth, which are crucial for improving osseointegration. These results underscore the potential of laser-assisted surface modification to optimize zirconia's performance as a medical implant material.

Keywords: zirconia; medical implant; laser patterning; confined plasma; sintering; surface modification

check for updates

Academic Editor: Rongwei Fan

Received: 22 November 2024
Revised: 21 December 2024
Accepted: 27 December 2024
Published: 2 January 2025

Citation: Majidov, I.; Allamyradov, Y.; Kylychbekov, S.; Khuzhakulov, Z.; Er, A.O. Phase Transition and Controlled Zirconia Implant Patterning Using Laser-Induced Shockwaves. *Appl. Sci.* **2025**, *15*, 362. https://doi.org/10.3390/app15010362

1. Introduction

Medical implants are essential in modern healthcare, and they address various conditions from joint replacements to dental and cardiovascular implants. The global medical implant market was valued at approximately $112.8 billion in 2023 and is projected to reach $225.7 billion by 2033 [1]. An aging population, advancements in medical technology, and the increasing prevalence of chronic diseases drive this growth. Titanium has long been the preferred material for medical implants, especially in orthopedic and dental applications. In 2023, 91.55% of the revenue in the $5 billion dental implant market was generated by titanium implants [2]. Its popularity stems from its excellent strength, durability, and biocompatibility. Biocompatibility refers to the ability of an implant to integrate into the body without causing adverse effects, such as inflammation or rejection, and is vital for the implant's stability and longevity. Additionally, biocompatibility is essential for osseointegration, the process by which the implant anchors to the bone, ensuring the implant's durability [3–5]. Titanium's biocompatibility ensures that it is not harmful to living tissues, and its high specific strength, excellent corrosion resistance, and ability to osseointegrate make it a reliable choice for long-term use [6,7]. However, titanium has some major drawbacks that necessitate the use of alternative materials, such as zirconia. In dentistry, patients often prefer more esthetically pleasing options, making titanium implants less suitable. Over time, titanium particles can be released from the implant surface via a process called tribocorrosion, the degradation of a material due to simultaneous mechanical wear and chemical or electrochemical corrosion, potentially causing inflammation and other adverse reactions [8]. It should be noted that, in rare instances, titanium particles released through tribocorrosion can induce localized adverse effects, such as inflammation or bone loss. These occurrences, although uncommon, highlight the importance of continued research into alternative materials for specific patient populations [9–11].

Zirconia implants have emerged as a promising alternative to titanium implants, particularly in dental applications [12–15]. Known for its esthetic superiority, zirconia is white and blends more naturally with teeth, unlike the grey tint of titanium. It also exhibits high corrosion resistance and is hypoallergenic, making it suitable for patients with metal allergies [16–18]. However, zirconia typically shows lower osseointegration compared to titanium, meaning that it does not integrate with bone as effectively, which can affect the long-term stability of the implant [19,20].

Zirconia implants typically show lower osseointegration compared to titanium implants due to differences in their surface properties [21]. Titanium's inherent roughness and ability to form a stable oxide layer provide a favorable environment for bone growth and integration [22]. In contrast, zirconia surfaces are smoother and chemically inert, which can limit cellular attachment and bone integration [23]. This limitation underscores the importance of surface modification techniques, such as laser-assisted template imprinting, to enhance zirconia's bioactivity and improve its osseointegration potential.

To enhance the biocompatibility of zirconia, we propose using laser-assisted template imprinting. This technique involves imprinting the shape of a grid template onto the surface via a shockwave produced from laser–material interaction. Studies have shown that topographical surface modifications can substantially alter a material's interaction with biological tissues by enhancing cell adhesion, protein adsorption, and bone-to-implant contact [24]. Increased surface area, surface roughness, and specific patterns promote better integration with the bone tissue [25–27]. Compared with other surface modification techniques, laser-assisted template imprinting offers precise control over surface characteristics, leading to enhanced osteoblast activity [28,29].

2. Materials and Methods

2.1. Preparation of Zirconia Sample

Zirconia pellets were prepared using MSE PRO Monoclinic Zirconium Oxide Nanoparticles, MSE Supplies LLC, Tucson, AZ, USA (20–40 nm in size) with a purity of over 99.9%. Zirconia powder was mixed with 5 wt% polyvinyl alcohol (PVA), which served as the binding agent. The mixture was then placed into a 13 mm-diameter hardened steel dry-pressing die set to form pellets at a maximum pressure of 8 MPa. Each zirconia pellet weighed 1 g and had a 13 mm diameter in its pressed form, referred to as a green body. After patterning, the samples were sintered in an MTI KSL-1500x (MTI Corporation, Richmond, CA, USA) furnace at 1450 °C. During sintering the pellet's diameter shrank to 10 mm due to densification. Phase transition from monoclinic zirconia (ρ = 5.68 g/cm^3) to tetragonal zirconia (ρ = 6.1 g/cm^3) results in increased density and particle diffusion.

Before patterning the pre-sintered zirconia samples, surface roughness was reduced to 0.05 µm using a Buehler EcoMet 250 Grinder-Polisher with an AutoMet 250 Powerhead (Buehler, Lake Bluff, IL, USA) [30]. Aluminum foil (Reynolds Wrap, Louisville, KY, USA) and graphite dry lubricant (Blasters, Tampa, FL, USA) were used as the sacrificial layers. Sizes of 100–2000 mesh-sized copper TEM grids were used as templates. A clean glass slide (Sargent Welch, New York, NY, USA) with 84% transmittance at 1064 nm served as a confinement medium [31]. The laser used for patterning was a 1064 nm, 10 Hz Nd-YAG pulsed laser with a pulse width of 5 ns, 225 Q-switch value, and a focused 3 mm-diameter Gaussian beam.

Once the grid patterns were imprinted, the sample was subjected to a sintering process. The sintering process was carefully managed to avoid pattern degradation or melting. To achieve this, a two-stage sintering procedure was implemented. The patterned green body will go through a two-step sintering, while the pre-sintered zirconia will go through a second step of sintering at 1450 °C [32]. The processes of pre-sintering at 1200 °C and complete sintering at 1450 °C are detailed in Table 1. The sintering process was developed after numerous trials to find the one with the best pattern retention. This controlled approach ensured that the patterns remained intact and consistent throughout sintering. The pre-sintering phase is especially important for preventing the patterns from deforming. Based on these findings, zirconia patterning requires careful attention to the material phase and the methods used. Zirconia is functional in the tetragonal phase and malleable only in the monoclinic phase. This change in the zirconia properties makes it a challenging task to find the form with the perfect mix of phases for the best pattern imprinting and retention. The success of the green body form of zirconia demonstrates that patterning at this stage is the most effective strategy.

Table 1. Sintering process for green body zirconia. Steps 1–6: pre-sintering; steps 7–12: sintering.

Step	Temperature (°C)	Heating Rate (°C/Min)	Time (Min)	Process Description
STEP 1 (PRE-SINTERING)	20 → 900	10	88	Heat from room temperature to 900 °C at 10 °C/min
STEP 2 (PRE-SINTERING)	900	-	20	Hold at 900 °C for 20 min
STEP 3 (PRE-SINTERING)	900 → 1200	10	30	Heat from 900 °C to 1200 °C at 10 °C/min
STEP 4 (PRE-SINTERING)	1200	-	120	Hold at 1200 °C for 120 min to allow densification
STEP 5 (COOLING)	1200 → 300	10	90	Cool from 1200 °C to 300 °C at 10 °C/min
STEP 6 (COOLING)	300 → RT	-	Natural	Cool naturally from 300 °C to room temperature (RT)
STEP 7 (SINTERING)	20 → 900	10	88	Heat from room temperature to 900 °C at 10 °C/min
STEP 8 (SINTERING)	900	-	20	Hold at 900 °C for 20 min
STEP 9 (SINTERING)	900 → 1450	10	55	Heat from 900 °C to 1450 °C at 10 °C/min
STEP 10 (SINTERING)	1450	-	120	Hold at 1450 °C for 120 min to allow sintering
STEP 11 (COOLING)	1450 → 300	10	115	Cool from 1450 °C to 300 °C at 10 °C/min
STEP 12 (COOLING)	300 → RT	-	Natural	Cool naturally from 300 °C to room temperature (RT)

2.2. Laser-Induced Plasma

Laser-induced template imprinting via nonthermal plasma is a precision surface modification technique that leverages laser–material interactions and plasma dynamics. The process involves the use of a nanosecond-pulsed, 1064 nm Nd:YAG laser operating at 10 Hz, coupled with a metal template and a confined plasma environment, to transfer template patterns onto zirconia surfaces [33].

The process begins with the laser pulse interacting with an ablative layer, typically made of aluminum or copper. These materials are selected for their excellent thermal and electrical conductivity, which ensures efficient absorption of laser energy. Upon irradiation, a thin layer of the template material undergoes rapid heating and vaporization, producing a nonthermal plasma [34]. The nonthermal plasma generated in this process plays a crucial role in efficient and localized energy transfer.

Unlike thermal plasmas, where all species are in thermal equilibrium, nonthermal plasmas have much higher electron temperatures compared to ions and neutrals. This temperature disparity arises because electrons, being lighter and more mobile, absorb and donetransfer energy more rapidly than their heavier counterparts. The electron temperature T_e is given by:

$$T_e = \frac{2}{3}\frac{E_e}{k_B}$$

where E_e is the average electron energy, and k_B is the Boltzmann constant. This disparity is a defining feature of nonthermal plasmas, enabling efficient energy localization during the imprinting process.

This characteristic enhances energy transfer efficiency and allows for precise surface modifications without excessive bulk heating. The generated plasma, composed of energetic ions, electrons, and neutral particles, is confined using a glass slide placed above the template. This confinement prevents the plasma from expanding freely, resulting in an increase in localized temperature and pressure. The confined plasma acts as a highly energetic medium, transferring its energy to the zirconia surface and inducing localized melting and ablation. This process enables the zirconia to conform precisely to the template's pattern under the combined thermal and mechanical effects of the plasma.

Key parameters governing the plasma and energy transfer include the laser's wavelength, pulse duration, and energy density. The 1064 nm wavelength is particularly effective due to its high absorption efficiency in metals like aluminum and copper, facilitating optimal plasma generation [35]. Additionally, the choice of nanosecond-pulse durations balances thermal and mechanical effects, providing sufficient energy for material processing while maintaining control over the heat-affected zone.

The absorbed laser energy (E) can be quantified as follows:

$$E = \int I(t)dt$$

$I(t)$ represents the laser intensity as a function of time [36]. The confined plasma pressure (P) is given by the following:

$$P = \frac{2E}{A \times t}$$

where A is the laser spot area, and t is the pulse duration [36]. Beam spot area (A) is a fixed value in this setup, as it should be irradiating the 3 mm template used for imprinting. The resulting high temperature and pressure induce localized melting and solidification of zirconia, ensuring the imprinting of precise patterns [37]. Upon cooling, the imprinted zirconia retains these patterns, which are characterized by techniques like AFM and SEM to evaluate their dimensions, uniformity, and depth.

2.3. Laser Shockwave Imprinting

Two similar approaches with different sacrificial layers were employed for the pattern imprinting [38]. In the first approach, a thin 10 μm layer of graphite was sprayed using a dry graphite lubricant to function as a sacrificial layer, to prevent melting and ablation of the sample. A TEM copper grid was then placed on top as a template and ablative layer. The entire setup was sealed with BK7 glass, which confined the plasma generated by the laser–ablative layer interaction. In the second method, aluminum foil was used as a sacrificial layer to protect the material surface from melting and direct laser contact [39]. A TEM copper grid was placed on the zirconia surface and covered by a single sheet of 16 μm-thick aluminum foil and a BK7 glass slide to seal the setup.

The prepared samples were irradiated under a 3 mm-diameter focused laser beam, forming plasma. Plasma forms when zirconia is heated to extremely high temperatures, causing it to vaporize and ionize. This ionization process strips electrons from atoms, creating a hot, electrically charged gas [37,40]. The plasma expansion on the ablative layer was contained using glass slides, creating a localized pressure of 9 GPa and a temperature spike of 6500 K at a laser fluence of 2 J/cm^2. Extreme pressure and temperature stamps the TEM grid, causing plastic deformation on the zirconia surface, resulting in an imprinted grid pattern on the surface [41]. For samples patterned using the first approach, the graphite layer was washed with acetone.

Surface morphology was studied using scanning electron microscopy (SEM, Jeol 6510LV, Tokyo, Japan), atomic force microscopy (AFM, Nanosurf Flex AFM, Liestal, Switzerland), and a drop shape analyzer. The laser parameters were optimized to control protrusion heights, ensuring the patterns achieved the desired depth and uniformity. These analyses provided a detailed view of the pattern quality and surface modifications achieved, helping to understand the effectiveness of laser-assisted template imprinting techniques.

3. Results

3.1. Phase Transitions in Zirconia

The XRD analysis of zirconia at different sintering stages provides insights into the phase transitions and structural changes. Zirconia exhibits polymorphism, meaning it has multiple phases that are stable within specific temperature ranges: cubic zirconia (c-ZrO_2) is stable above 2370 °C, tetragonal zirconia (t-ZrO_2) between 1170 °C and 2370 °C, and monoclinic zirconia (m-ZrO_2) below 1170 °C [42]. To stabilize the tetragonal and cubic phases of zirconia at room temperature, it is doped with trace amounts of yttria.

Figure 1 displays the XRD patterns of zirconia in three forms: green, pre-sintered, and sintered. The hydrophobicity measurements for the green body, pre-sintered, and sintered samples, using a drop shape analyzer and young modulus, had shown 0°, 60°, and 82° contact angles, respectively, giving insight into the porosity and surface modifications happening. As expected, the XRD pattern of green body zirconia shows a pure monoclinic phase, with no distinct peaks at other phases. The pre-sintered sample shows a mixture of monoclinic and tetragonal zirconia. Figure 1 shows that the phase transition was observed, as evidenced by the change in peak intensities in the X-ray diffraction (XRD) patterns, with a decrease in the intensity of the monoclinic phase peaks and a corresponding increase in the intensity of the tetragonal phase peaks. Such transitions are significant in zirconia ceramics because the balance between monoclinic and tetragonal phases strongly influences the material's mechanical properties, including fracture toughness and strength. Repeating sintering with a faster cooling rate increases tetragonal phase retention, indicating that the cooling rate influences the phase transition, and rapid cooling favors phase retention. Other factors affecting phase transition and retention are the uneven distribution of yttria and yttria evaporation. The XRD pattern of fully sintered zirconia shows a pure tetragonal phase, confirming the total phase transition from monoclinic zirconia. This transformation is consistent with zirconia's phase stability, where the tetragonal phase is the most stable between 1170 °C and 2370 °C. The full phase transition in the sintered sample shows that the sintering temperature of 1450 °C provides enough energy for zirconia to completely convert from the monoclinic to the tetragonal phase. The sharp, high-intensity tetragonal peaks in the XRD pattern confirm the crystallinity and purity of the tetragonal phase. These observations are consistent with the theory of zirconia polymorphism. When monoclinic zirconia is heated above 1170 °C, it transitions to the tetragonal phase, where it undergoes a martensitic transformation involving significant volume change and shear strain.

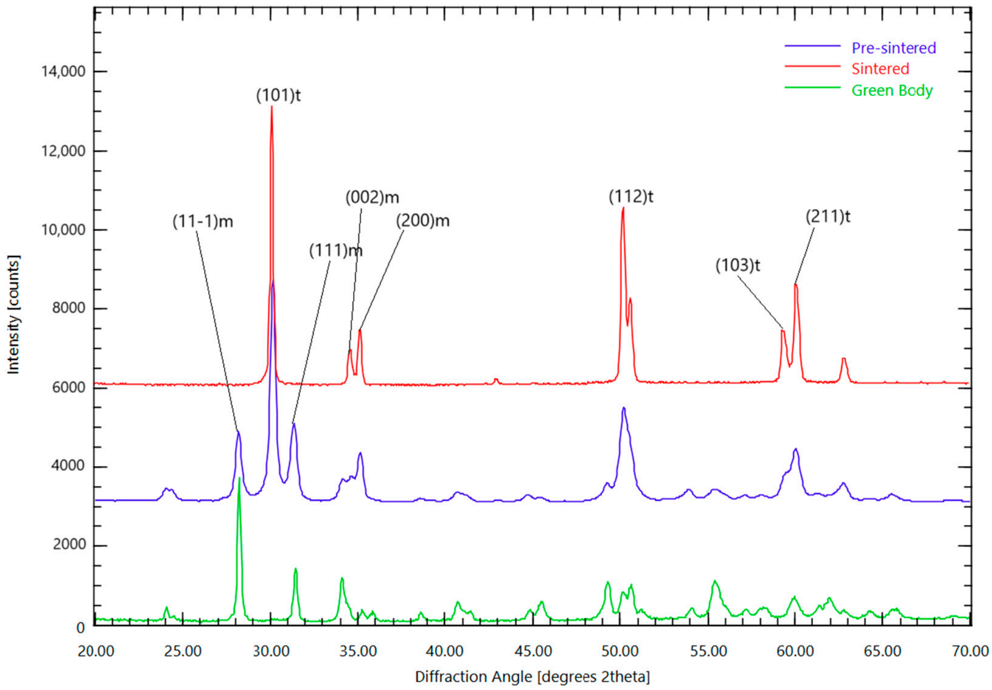

Figure 1. XRD pattern of zirconia. Sintered (red), pre-sintered (green), and green body (blue) ZrO_2 XRD profiles.

3.2. Laser Pattern Imprinting on Zirconia

The sintered properties of zirconia, particularly its high compressive strength, inherent hardness, and brittleness, create substantial obstacles to deformation under pressure. These attributes make patterning attempts exceedingly difficult, as the material's resistance to mechanical alteration often exceeds the capabilities of conventional patterning techniques. Unlike metals that deform plastically, zirconia tends to fracture because of its Hugoniot elastic limit (HEL) of 20–25 GPa [43]. Recognizing tetragonal zirconia's hardness, we tried green body and pre-sintered zirconia, seeking a balance between malleability for patterning and robustness to prevent fracturing. The two critical factors to consider are pattern retention and pattern precision. Sintered zirconia offers the highest pattern retention, whilst leaving much to be desired for pattern precision. The opposite is true for green body zirconia. Thus, finding a middle ground is an ideal case scenario. During our trials, the green body zirconia produced the best results, as the two-stage sintering improved pattern retention. Thus, we found green body zirconia to be the primary candidate for patterning.

Figure 2 shows SEM images illustrating the square grid pattern achieved on a zirconia pellet surface. Initially smooth and unblemished, the zirconia surface was patterned using the first method, which used graphite as a sacrificial layer. We administered a 1.2 J/cm^2 laser shot for 2 s, aiming for a uniform and reproducible pattern with high fidelity. The results show a clean imprint of the grid template. Elemental analysis of the grid square and pitch revealed similar compositions, containing zirconia and oxygen, as expected. The use of graphite in this method makes it unsuitable for sensitive fields such as medical implants. Nevertheless, this technique has shown promise in patterning on copper and titanium plates, where the precision and cleanliness of the imprint are less critical. The alternative approach uses aluminum as the ablative layer, making it more suitable for sensitive applications. Aluminum as a sacrificial layer facilitates a clearer, more precise imprint on the surface, without leaving any trace (see Figure 3).

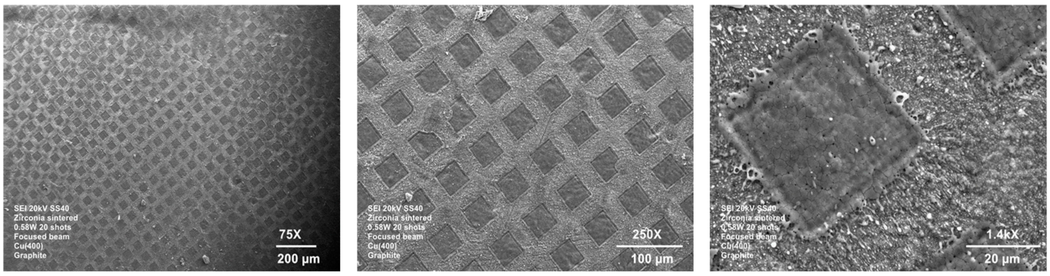

Figure 2. ZrO_2 patterned via the "graphite method". Cu (400) mesh TEM grid template at F = 1 J/cm^2, t = 2 s.

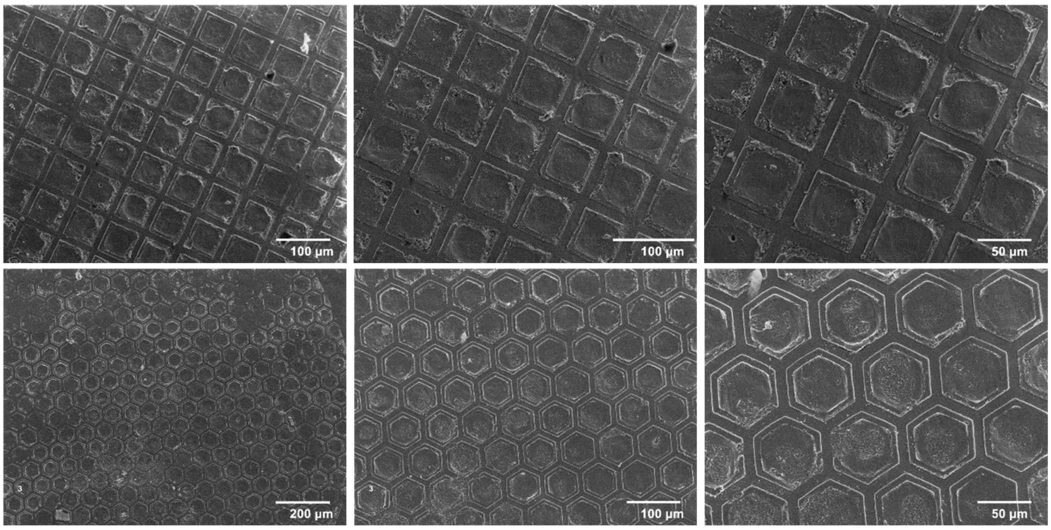

Figure 3. Zirconia surface patterned via the "aluminum method". First row: Cu (400) square mesh TEM template at F = 2 J/cm^2, t = 1 s. Second row: Cu (400) hexagonal mesh grid TEM template at F = 2 J/cm^2, t = 1 s.

SEM and AFM images of zirconia patterned via laser template imprinting reveal a highly precise and well-defined pattern. The SEM images show the uniformity and clarity of the imprinted patterns, highlighting the effectiveness of the proposed technique. The AFM images further support these findings, demonstrating excellent imprinting quality with clear and distinct features (see Figure 4). Notably, the depth profile observed in the AFM images is significantly deeper than that typically achievable with other laser-patterning methods, such as femtosecond pulsed laser irradiation and direct laser interference patterning (DLIP) [44,45]. These methods, while effective in creating precise microstructures and nanoscale periodic surface structures, often do not achieve the same depth and intricacy as nanosecond laser template imprinting. This enhanced depth profile is particularly important for zirconia implants because it promotes better osseointegration by increasing the surface area, which allows for stronger and more stable integration with the bone [46,47]. In addition, deeper patterns improve mechanical stability by providing better mechanical interlocking, reducing the risk of implant loosening or failure. They also help distribute mechanical stress more evenly, reducing the likelihood of fractures. Furthermore, deeper patterns enhance biocompatibility by providing a favorable environment for cell attachment and proliferation. Overall, the combination of SEM and AFM analyses provides a comprehensive understanding of the high-quality patterning achieved through laser template imprinting on zirconia.

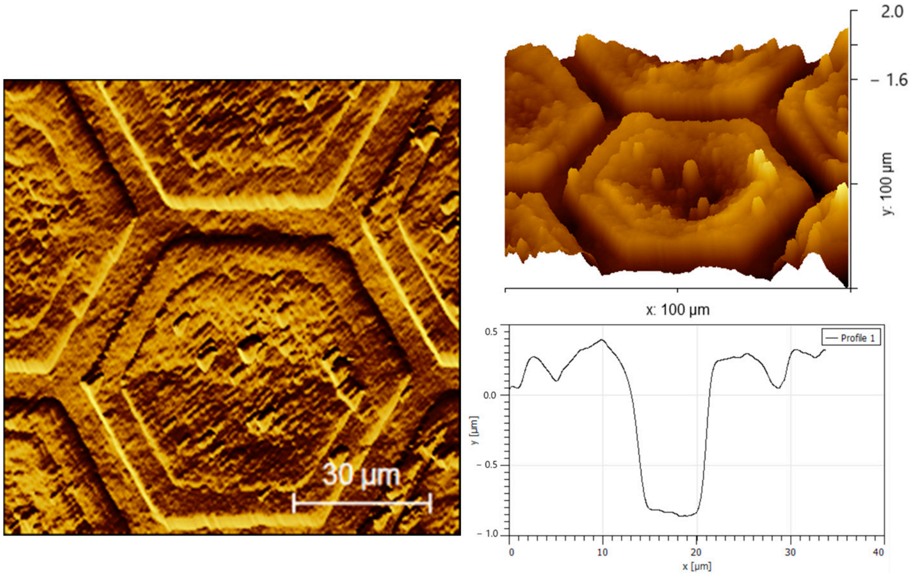

Figure 4. AFM image, 3D image, and depth profile plot of a patterned zirconia via the aluminum method. Cu(400) hexagonal mesh grid TEM template at F = 2 J/cm^2, t = −1 s.

3.3. Bioanalysis via Protein Adsorption

In this study, our focus was on enhancing the biocompatibility of zirconia implants, with a particular emphasis on osseointegration. Osseointegration, which is crucial for the success of zirconia implants, refers to the formation of a stable bond between living bone tissue and the implant surface. Given the challenges associated with directly measuring osseointegration, we used protein adsorption as an indirect indicator. Specifically, we conducted a protein adsorption experiment using bovine serum albumin (BSA) to better understand the osseointegration process and to draw indirect correlations [48,49].

The adsorption study was conducted under three surface conditions: 27% patterned surface coverage (Sample 1), 36% patterned surface coverage (Sample 2), and a non-patterned control. The absorbance measurements, which indicate the amount of light absorbed by the protein in solution, were used to determine the amount of protein adsorbed onto the surface. In this analysis, lower absorbance values correspond to higher levels of protein adsorption on the surface. Figure 5 illustrates absorbance trends over time, with the calculated slopes for Sample 2, Sample 1, and the untreated control determined to be 2.6×10^{-3}, 5×10^{-3}, and 7×10^{-3}, respectively. The results indicate that Sample 1 exhibited a 92% increase in adsorption relative to the reference sample, while Sample 2 exhibited a 169% increase. These data demonstrate a direct relationship between surface pattern coverage and adsorption rate, validating the hypothesis that surface patterning enhances protein adsorption. These findings indicate that a higher degree of surface patterning supports improved osseointegration, as shown by increased protein adsorption.

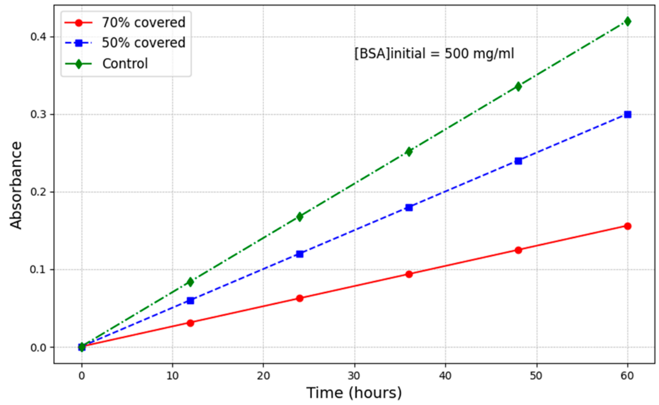

Figure 5. BSA absorbance as a function of time at 562 nm.

4. Discussion

The results of this study demonstrate the effectiveness of laser-assisted template imprinting in enhancing the osseointegration of zirconia implants. The phase transition analysis highlighted the critical role of sintering temperature and cooling rates in achieving a stabilized tetragonal phase, essential for the implants' mechanical properties and biocompatibility [50,51]. By stabilizing tetragonal zirconia before the imprint patterning, we were able to avoid the issues with phase degradation reported in other studies, such as femtosecond LIPSS [52].

Our findings revealed that green body zirconia offered the best balance between imprint precision and pattern retention during laser patterning, addressing the reported issues of low fidelity observed in fully sintered zirconia due to its surface brittleness and hardness [53]. The transition from graphite to aluminum as a sacrificial layer significantly improved pattern quality, making it suitable for sensitive applications like medical implants.

Furthermore, protein adsorption studies confirmed a direct correlation between increased surface pattern coverage and enhanced bioactivity, as evidenced by the notable 92% increase in protein adsorption for a patterned surface compared to the unpatterned control. The increase in protein adsorption for the patterned area aligns with the finding from studies on LIPSS patterning and sandblasting [46]. Beyond the primary outcomes, the study revealed several secondary insights. The combination of SEM and AFM analyses validated the precision and depth of the patterns achieved through laser-assisted template imprinting, which were superior to other techniques like direct laser interference patterning and nanosecond laser-induced periodic surface structuring [44,45]. These deeper and more intricate patterns are critical for promoting better osseointegration and mechanical stability by providing enhanced surface area and interlocking capabilities. Additionally, the hydrophobicity measurements aligned with the phase transition observations, illustrating improved wettability with surface modifications. These findings align with the existing research that shows wettability to improve protein interaction and osteoblast activity [51]. The comparison of sacrificial layers also provided valuable information on optimizing the imprinting process for different applications.

The findings of this study align with and extend previous research on surface modifications to enhance the bioactivity of zirconia implants. While earlier studies have explored techniques like direct laser interference patterning and femtosecond laser irradiation, our approach of laser-assisted template imprinting offers a more precise and reproducible method for achieving intricate patterns. Unlike traditional methods, our use of a confined plasma environment and optimized sacrificial layers significantly improves the quality and fidelity of the imprints. These advancements directly contribute to the growing body of literature supporting the use of surface patterning as a strategy to enhance osseointegration and biocompatibility in zirconia implants.

Despite these promising results, the study has certain limitations that warrant consideration. The research focused on in vitro analyses, and the findings must be validated through in vivo studies to confirm their clinical relevance. Additionally, while the protein adsorption experiments provided indirect evidence of enhanced osseointegration, direct measurements, such as bone-to-implant contact analysis, are needed for a comprehensive evaluation. Future research should also explore the long-term stability of the imprinted patterns under physiological conditions and investigate the scalability of the laser-assisted template imprinting technique for commercial applications. Lastly, expanding the study to include different zirconia compositions and implant geometries could provide further insights into the generalizability of the findings.

5. Conclusions

In this study, we investigated the phase transitions and laser patterning of zirconia implants to enhance their performance. Our results demonstrate that laser-assisted template imprinting significantly improves protein adsorption and osseointegration, with a 92% increase for 27% surface coverage and a 169% increase for 36% surface coverage. These improvements are attributed to precise and uniform surface patterns that promote better integration with bone tissue. The findings on phase transitions during sintering and the optimization of patterning techniques offer a basis for advancing zirconia implants. While promising, further in vivo studies are needed to confirm the clinical benefits and long-term efficacy of these implants. Future research will refine these processes and explore additional materials for improved biomedical solutions.

Author Contributions: Conceptualization, A.O.E.; methodology, I.M., Y.A., S.K., Z.K. and A.O.E.; formal analysis, I.M., Y.A. and A.O.E.; investigation, I.M., Y.A., S.K., Z.K. and A.O.E.; writing—original draft preparation, I.M.; writing—review and editing, A.O.E.; project administration, A.O.E.; funding acquisition, A.O.E. All authors have read and agreed to the published version of the manuscript.

Funding: This project is fully supported by Kentucky Biomedical Research Infrastructure Network and INBRE (KBRIN) 5P20GM 103436-23 and NSF MRI (Award Number 1920069), WKU RCAP, and KY NSF EPSCoR RA (#3200002692-23-011).

Institutional Review Board Statement: Not applicable.

Informed Consent Statement: Not applicable.

Data Availability Statement: The original contributions presented in this study are included in the article. Further inquiries can be directed to the corresponding author.

Acknowledgments: We would like to thank John Andersland for his invaluable technical assistance and expert guidance throughout this project.

Conflicts of Interest: The authors declare no conflicts of interest.

References

1. Research, A.M. Medical Implant Market to Reach $225.7 Billion by 2033 | Conmed Corporation, Globus Medical, Inc., Institut St. 2024. Available online: https://www.openpr.com/news/3714920/medical-implant-market-to-reach-225-7-billion-by-2033-conmed (accessed on 12 November 2024).
2. Dental Implants Market Size, Share and Growth Report 2030. Available online: https://www.grandviewresearch.com/industry-analysis/dental-implants-market (accessed on 13 November 2024).
3. Elias, C.N.; Meirelles, L. Improving Osseointegration of Dental Implants. *Expert. Rev. Med. Devices* **2010**, *7*, 241–256. [CrossRef] [PubMed]

4. Albrektsson, T.; Johansson, C. Osteoinduction, osteoconduction and osseointegration. *Eur. Spine J.* **2001**, *10*, S96–S101. [CrossRef] [PubMed]
5. Parithimarkalaignan, S.; Padmanabhan, T.V. Osseointegration: An Update. *J. Indian Prosthodont. Soc.* **2013**, *13*, 2–6. [CrossRef]
6. Takadoum, J. Review on Corrosion, Tribocorrosion and Osseointegration of Titanium Alloys as Biomaterials. *Corros. Mater. Degrad.* **2023**, *4*, 644–658. [CrossRef]
7. Sun, X.-D.; Liu, T.-T.; Wang, Q.-Q.; Zhang, J.; Cao, M.-S. Surface Modification and Functionalities for Titanium Dental Implants. ACS Biomater. *Sci. Eng.* **2023**, *9*, 4442–4461. [CrossRef]
8. Zhang, Z.; Dandu, R.S.B.; Klu, E.E.; Cai, W. A Review on Tribocorrosion Behavior of Aluminum Alloys: From Fundamental Mechanisms to Alloy Design Strategies. *Corros. Mater. Degrad.* **2023**, *4*, 594–622. [CrossRef]
9. Kitagawa, M.; Murakami, S.; Akashi, Y.; Oka, H.; Shintani, T.; Ogawa, I.; Inoue, T.; Kurihara, H. Current status of dental metal allergy in Japan. *J. Prosthodont. Res.* **2019**, *63*, 309–312. [CrossRef] [PubMed]
10. Albrektsson, T.; Chrcanovic, B.; Mölne, J.; Wennerberg, A. Foreign body reactions marginal bone loss allergies in relation to titanium implants. *Eur. J. Oral. Implantol.* **2018**, *11* (Suppl. 1), S37–S46. [PubMed]
11. Comino-Garayoa, R.; Cortés-Bretón Brinkmann, J.; Peláez, J.; López-Suárez, C.; Martínez-González, J.M.; Suárez, M.J. Allergies to Titanium Dental Implants: What Do We Really Know about Them? A Scoping Review. *Biology* **2020**, *9*, 404. [CrossRef]
12. Özkurt, Z.; Kazazoğlu, E. Zirconia Dental Implants: A Literature Review. *J. Oral Implant.* **2011**, *37*, 367–376. [CrossRef] [PubMed]
13. Osman, R.; Swain, M. A Critical Review of Dental Implant Materials with an Emphasis on Titanium versus Zirconia. *Materials* **2015**, *8*, 932–958. [CrossRef]
14. Apratim, A.; Eachempati, P.; Krishnappa Salian, K.; Singh, V.; Chhabra, S.; Shah, S. Zirconia in Dental Implantology: A Review. *J. Int. Soc. Prev. Community Dent.* **2015**, *5*, 147. [CrossRef]
15. Thu, M.K.; Kang, Y.S.; Kwak, J.M.; Jo, Y.-H.; Han, J.-S.; Yeo, I.-S.L. Comparison between bone–implant interfaces of microtopographically modified zirconia and titanium implants. *Sci. Rep.* **2023**, *13*, 11142. [CrossRef] [PubMed]
16. Zarzar, A.A. Immunologically Neutral Dental Implants Ceramic (Zirconia) Implants. *J. Dent. Oral. Sci.* **2022**, *4*, 1–22. [CrossRef]
17. Monti, L.; Franchi, M.; Ursino, N.; Mariani, I.; Corona, K.; Anghilieri, F.M.; D'Ambrosi, R. Hypoallergenic Unicompartmental Knee Arthroplasty and Return to Sport: Comparison between Oxidized Zirconium and Titanium Niobium Nitride. *Acta Biomed. Atenei Parm.* **2022**, *93*, 2022160. [CrossRef]
18. Bollen, C.; Hakobayan, G.; Jörgens, M. One-piece versus two-piece ceramic dental implants. *Br. Dent. J.* **2024**, *236*, 383–387. [CrossRef]
19. Bosshardt, D.D.; Chappuis, V.; Buser, D. Osseointegration of Titanium, Titanium Alloy and Zirconia Dental Implants: Current Knowledge and Open Questions. *Periodontology* **2000**, *73*, 22–40. [CrossRef]
20. Depprich, R.; Zipprich, H.; Ommerborn, M.; Naujoks, C.; Wiesmann, H.-P.; Kiattavorncharoen, S.; Lauer, H.-C.; Meyer, U.; Kübler, N.R.; Handschel, J. Osseointegration of Zirconia Implants Compared with Titanium: An in Vivo Study. *Head. Face Med.* **2008**, *4*, 30. [CrossRef]
21. Hanawa, T. Zirconia versus Titanium in Dentistry: A Review. *Dent. Mater. J.* **2020**, *39*, 24–36. [CrossRef] [PubMed]
22. Stich, T.; Alagboso, F.; Křenek, T.; Kovářík, T.; Alt, V.; Docheva, D. Implant-bone-interface: Reviewing the impact of titanium surface modifications on osteogenic processes in vitro and in vivo. *Bioeng. Transl. Med.* **2021**, *7*, e10239. [CrossRef] [PubMed]
23. Pae, A.; Lee, H.; Noh, K.; Woo, Y.-H. Cell attachment proliferation of bone marrow-derived osteoblast on zirconia of various surface treatment. *J. Adv. Prosthodont.* **2014**, *6*, 96. [CrossRef] [PubMed]
24. Ahrens, M.; Spörer, M.; Deppe, H.; Ritschl, L.M.; Mela, P. Bacterial reduction and temperature increase of titanium dental implant models treated with a 445 nm diode laser: An in vitro study. *Sci. Rep.* **2024**, *14*, 18053. [CrossRef]
25. Shayeb, M.A.; Elfadil, S.; Abutayyem, H.; Shqaidef, A.; Marrapodi, M.M.; Cicciù, M.; Minervini, G. Bioactive surface modifications on dental implants: A systematic review and meta-analysis of osseointegration and longevity. *Clin. Oral Investig.* **2024**, *28*, 592. [CrossRef] [PubMed]
26. Chakravorty, N.; Jaiprakash, A.; Ivanovski, S.; Xiao, Y. Implant Surface Modifications and Osseointegration. In *Biomaterials for Implants and Scaffolds*; Li, Q., Mai, Y.-W., Eds.; Springer: Berlin/Heidelberg, Germany, 2017; pp. 107–131.
27. Pellegrini, G.; Francetti, L.; Barbaro, B.; Del Fabbro, M. Novel Surfaces and Osseointegration in Implant Dentistry. *J. Investig. Clin. Dent.* **2018**, *9*, 12349. [CrossRef] [PubMed]
28. Daskalova, A.; Ostrowska, B.; Zhelyazkova, A.; Święszkowski, W.; Trifonov, A.; Declercq, H.; Nathala, C.; Szlazak, K.; Lojkowski, M.; Husinsky, W.; et al. Improving osteoblasts cells proliferation via femtosecond laser surface modification of 3D-printed poly-ε-caprolactone scaffolds for bone tissue engineering applications. *Appl. Phys. A.* **2018**, *124*, 413. [CrossRef]
29. Hao, L.; Lawrence, J.; Chian, K.S. Osteoblast Cell Adhesion on a Laser Modified Zirconia Based Bioceramic. *J. Mater. Sci. Mater. Med.* **2005**, *16*, 719–726. [CrossRef]
30. Metallographic Specimen Preparation for Zirconia Ceramics. Available online: https://www.metallographic.com/Metallographic-Preparation-Procedures/Zirconia-ceramic (accessed on 13 November 2024).
31. Creasey, D.; Akkus, O. 1064-nm Raman: The right choice for biological samples? *Spectroscopy* **2017**, *32*, 46–54.

32. Zirconia Dentures-Beautyzir 3DPro Multilayer 98mm-Full Crown Bridges—Beautyzir Dental. Available online: https://www.beautyzir.com/products/3dpro-multilayer-98mm (accessed on 13 November 2024).
33. Jin, S. Laser Shock Imprinting of Metallic Membranes Toward Soft Templates and Its Applications. Ph.D. Thesis, Purdue University, West Lafayette, IN, USA, 2019; pp. 1–106.
34. Duchateau, G.; Hu, S.X.; Pineau, A.; Kar, A.; Chimier, B.; Casner, A.; Tikhonchuk, V.; Goncharov, V.N.; Radha, P.B.; Campbell, E.M. Modeling the solid-to-plasma transition for laser imprinting in direct-drive inertial confinement fusion. *Phys. Rev. E* **2019**, *100*, 033201. [CrossRef]
35. Liu, T.; Gao, X.; Hao, Z.; Liu, Z.; Lin, J. Characteristics of plasma plume expansion from Al target induced by oblique incidence of 1064 and 355 nm nanosecond Nd: YAG laser. *J. Phys. Appl. Phys.* **2013**, *46*, 485207. [CrossRef]
36. Colvin, J.; Larsen, J. *Extreme Physics: Properties and Behavior of Matter at Extreme Conditions*; Cambridge University Press: Cambridge, UK, 2013.
37. Ilhom, S.; Kholikov, K.; Li, P.; Ottman, C.; Sanford, D.; Thomas, Z. Scalable patterning using laser-induced shock waves. *Opt. Eng.* **2018**, *57*, 041413. [CrossRef]
38. Majidov, I.; Allamyradov, Y.; Kylychbekov, S.; Khuzhakulov, Z. Surface patterning on zirconia dental implants by laser imprinting. In *Laser-Based Micro- and Nanoprocessing XVIII*; Kling, R., Pfleging, W., Sugioka, K., Eds.; SPIE: San Francisco, CA, USA, 2024; p. 56.
39. Wang, L.; Su, C.; Jia, X.; Guo, Z.; Zou, Z. Experiment and Simulation Study of the Laser-Induced Cavitation Bubble Technique for Forming a Microgroove in Aluminum Foil. *Micromachines* **2023**, *14*, 2106. [CrossRef] [PubMed]
40. Pustovalov, V.K. Heating of nanoparticles and their environment by laser radiation and applications. *Nanotechnol. Precis. Eng.* **2024**, *7*, 015001. [CrossRef]
41. Yang, R.; Hu, Y. Plastic deformation mechanisms and their threshold pressures of Ti6Al4V thin-walled structures induced by laser peen forming. *Opt. Laser Technol.* **2023**, *167*, 109722. [CrossRef]
42. Peyre, P.; Berthe, L.; Scherpereel, X.; Fabbro, R.; Bartnicki, E. Experimental study of laser-driven shock waves in stainless steels. *J. Appl. Phys.* **1998**, *84*, 5985–5992. [CrossRef]
43. Cutler, R.A.; Reynolds, J.R.; Jones, A. Sintering and Characterization of Polycrystalline Monoclinic, Tetragonal, and Cubic Zirconia. *J. Am. Ceram. Soc.* **1992**, *75*, 2173–2183. [CrossRef]
44. Mulko, L.; Soldera, M.; Lasagni, A.F. Structuring and functionalization of non-metallic materials using direct laser interference patterning: A review. *Nanophotonics* **2022**, *11*, 203–240. [CrossRef] [PubMed]
45. Khuzhakulov, Z.; Kylychbekov, S.; Allamyradov, Y.; Majidov, I.; Ben Yosef, J.; Er, A.Y.; Kitchens, C.; Banga, S.; Badarudeen, S.; Er, A.O. Formation of picosecond laser-induced periodic surface structures on steel for knee arthroplasty prosthetics. *Front. Met. Alloys* **2023**, *1*, 1090104. [CrossRef]
46. Jin, H.W.; Noumbissi, S.; Wiedemann, T.G. Comparison of Zirconia Implant Surface Modifications for Optimal Osseointegration. *J. Funct. Biomater.* **2024**, *15*, 91. [CrossRef] [PubMed]
47. Zhang, W.; Fu, W.; Wang, X.; Ye, J. Improving the osseointegration soft tissue sealing of zirconia ceramics by the incorporation of akermanite via sol infiltration for dental implants. *J. Mater. Chem. B* **2023**, *11*, 4237–4259. [CrossRef] [PubMed]
48. Putman, B.; Van Der Meeren, P.; Thierens, D. Reduced bovine serum albumin adsorption by prephosphatation of powdered zirconium oxide. *Colloids Surf. Physicochem. Eng. Asp.* **1997**, *121*, 81–88. [CrossRef]
49. Fathi, A.; Asgari, E.; Danafar, H.; Salehabadi, H.; Fazli, M.M. A comprehensive study on methylene blue removal via polymer and protein nanoparticle adsorbents. *Sci. Rep.* **2024**, *14*, 29434. [CrossRef] [PubMed]
50. Sun, L.; Hong, G. Surface Modifications for Zirconia Dental Implants: A Review. *Front. Dent. Med.* **2021**, *2*, 733242. [CrossRef]
51. Lin, H.; Yin, C.; Mo, A. Zirconia Based Dental Biomaterials: Structure, Mechanical Properties, Biocompatibility, Surface Modification, and Applications as Implant. *Front. Dent. Med.* **2021**, *2*, 689198. [CrossRef]
52. Cunha, W.; Carvalho, O.; Henriques, B.; Silva, F.S.; Özcan, M.; Souza, J.C.M. Surface modification of zirconia dental implants by laser texturing. *Lasers Med. Sci.* **2022**, *37*, 77–93. [CrossRef] [PubMed]
53. da Cruz, M.B.; Marques, J.F.; Marques, A.F.S.; Madeira, S.; Carvalho, Ó.; Silva, F.; Caramês, J.; da Mata, A.D.S.P. Modification of Zirconia Implant Surfaces by Nd:YAG Laser Grooves: Does It Change Cell Behavior? *Biomimetics* **2022**, *7*, 49. [CrossRef]